Engineering Optimization

ISSN: (Print) (Online) Journal homepage: https://www.tandfonline.com/loi/geno20

Adjoint-based optimization in the development of low-emission industrial boilers

Georgios Kanellis , Antti Oksanen & Jukka Konttinen

To cite this article: Georgios Kanellis , Antti Oksanen & Jukka Konttinen (2020): Adjoint-based optimization in the development of low-emission industrial boilers, Engineering Optimization, DOI: 10.1080/0305215X.2020.1781842

To link to this article: https://doi.org/10.1080/0305215X.2020.1781842

Published online: 16 Jul 2020.

ENGINEERING OPTIMIZATION
https://doi.org/10.1080/0305215X.2020.1781842

Taylor & Francis
Taylor & Francis Group

Adjoint-based optimization in the development of low-emission industrial boilers

Georgios Kanellis, Antti Oksanen and Jukka Konttinen

Faculty of Engineering and Natural Sciences, Tampere University, Tampere, Finland

ABSTRACT

A gradient-based method has been developed and programmed to optimize the NH_3 injections of an existing biomass-fired bubbling fluidized bed boiler, the targets being to minimize both the NO and the NH_3 emissions. In this context, the reactive flow inside the boiler is modelled using a custom-built OpenFOAM® solver, and then the NO and NH_3 species are calculated using a post-processing technique. The multiobjective optimization problem is solved by optimizing several weight combinations of the objectives using the gradient-projection method. The required sensitivities were calculated by differentiating the post-processing solver according to the discrete adjoint method. The adjoint-based sensitivities are validated against finite differences calculations. Moreover, in order to evaluate the optimization results, the optimization problem is solved using evolutionary algorithms software. Finally, the optimization results are physically interpreted and the strengths and weaknesses of the proposed method are discussed.

ARTICLE HISTORY
Received 6 September 2019
Accepted 9 June 2020

KEYWORDS
CFD; optimization; adjoint; boiler; emissions

1. Introduction

NO_x emissions have become a major environmental issue, especially in highly industrialized countries, since they contribute to the formation of photochemical smog and acid rain, as well as ground level ozone, which is a dangerous pollutant. This fact provoked political action and the implementation of restrictive legislation in order to reduce nitric oxide (NO) emissions. As a consequence, recently, in the field of industrial combustion, several studies have been made aiming at the systematic optimization of various boiler design parameters for low NO_x operation.

A few of those used Computational Fluid Dynamics (CFD) in order to model the NO_x emissions in combination with a derivative-free search method. Risio *et al.* (2005) conducted one of the first studies combining CFD combustion modelling with evolutionary-algorithm-based optimization in order to optimize NO_x and carbon burnout in boilers. In addition, Saario and Oksanen (2008) used evolutionary algorithms and CFD modelling in order to optimize the NH_3 and NO emissions of a bubbling fluidized bed boiler. Dal Secco *et al.* (2015) used a genetic algorithm combined with CFD in order to identify low NO_x configurations in an industrial boiler. Salahi (2012) optimized NO_x and CH_4 emissions of a coal combustion reactor using the ε-constraint method combined with the SIMPLEX method for the resulting Single Objective Optimization (SOO) problems and CFD modelling as the evaluation tool.

In general, similar methods have also been used extensively in the broader field of combustion optimization. For example, Janiga and Thévenin (2007) reduced the CO emissions in a laminar burner

CONTACT G. Kanellis georgios.kanellis@tuni.fi

using genetic algorithms and also the SIMPLEX method. Also, Liu and Bansal (2014) improved a boiler's heat transfer while at the same time decreasing the probabilities for slagging by combining the multiobjective optimization NSGA algorithm with CFD modelling.

From the above it can be seen that systematic combustion optimization is usually performed using derivative-free (and stochastic in most cases) optimization algorithms. While those algorithms usually converge to the desired optima, they are rather slow when compared with Gradient-Based Methods (GBMs), which in turn add an extra complexity to the process owing to the need for the calculation of the sensitivity derivatives of the objective function(s) with respect to the design variables. In CFD-based optimization, the adjoint method has proven to be an efficient way to compute the sensitivity derivatives—see *e.g.* Chapter 4 of Thévenin and Janiga (2008). This method is introduced in Pironneau (1982) for elliptic problems and then further extended in several publications by Jameson for potential, inviscid and viscous flow equations (Jameson 1988; Jameson and Reuther 1994; Jameson, Martinelli, and Pierce 1998). There are two approaches for the construction of the adjoint equations: (1) the discrete, in which the discretized form of the PDEs is differentiated; and (2) the continuous, in which the adjoint differential equations are first formed from the PDEs in their continuous form and then discretized and solved. For more information on the differences between the discrete and the continuous adjoint approaches, see *e.g.* Nadarajah and Jameson (2000) and Giles and Pierce (2000).

In the field of reactive flows, the continuous adjoint method has been applied recently by Braman, Oliver, and Raman (2015) to calculate the sensitivities of laminar flames to several chemistry and fluid model parameters. In addition, Lemke, Reiss, and Sesterhenn (2014) applied the continuous adjoint method in order to optimize 1-D and 2-D flame configurations.

The target of this article is to utilize the discrete adjoint method in the context of a gradient-based method in order to reduce the NO and NH_3 emissions of a Bubbling Fluidized Bed Boiler (BFBB), which was previously optimized in Saario and Oksanen (2008) using Evolutionary algorithms. To the authors' knowledge this is one of the first applications of the adjoint method in industrial boiler environments.

To this end, the reactive flow in the BFBB is modelled using a solver based on the OpenFOAM® (Weller *et al.* 1998) libraries. The emissions are calculated by solving the Nitrogen species' transport equations in a post processing fashion. Then, the post processing solver is differentiated and the sensitivity derivatives with respect to the design variables are computed using the discrete adjoint method. For the optimization, a gradient-based algorithm, the gradient-projection method, is implemented. In addition, the emission minimization problem is solved again using evolutionary algorithms, also proposing several improvements over Saario and Oksanen (2008), and the solutions obtained with the different optimization methods are compared. Finally, the optimization results are physically interpreted and the strengths and weaknesses of the proposed method in terms of computational time are discussed.

2. Case description

The bubbling fluidized bed is a combustion technology used to burn low quality (*i.e.* high moisture and ash content, low calorific value) fuel efficiently. In a Bubbling Fluidized Bed Boiler (BFBB) the lower part consists of a bed of silica sand particles of about 0.5–1 mm in diameter. The primary air is fed upwards through the bottom of the bed with a velocity between 1 and 2 m/s, so that the bed material and other solids remain mainly in the bottom part of the furnace.

In this study, a BFBB burning mainly biomass sludge and a small amount of plastic reject is modelled (Figure 1). In addition, a small amount of methane (CH_4) is injected into the boiler as supporting fuel. The boiler has a capacity of 40 MW_{th}, a height of approximately 18 m and a bed area of about 50 m^2. The primary air is fed through the bed. The secondary air injections are at the level of 3.6 m and three fuel feeds are at the level of 2.83 m.

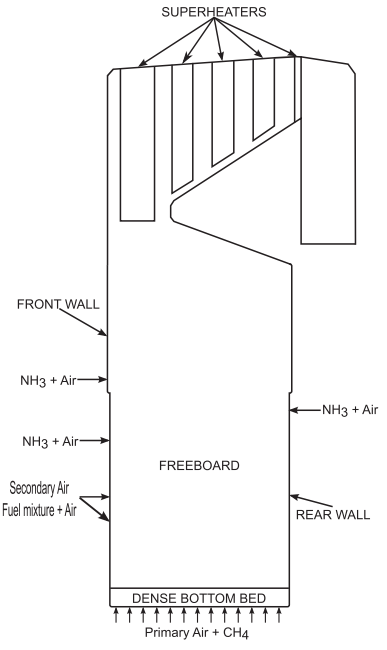

Figure 1. Modelled boiler geometry.

Usually, those boilers are supplied with a Selective Non-Catalytic Reduction (SNCR) system, which is a post combustion system for NO_x abatement. The SNCR system consists of several nozzles which inject NH_3 into the flue gas in order to react with NO, the main products being harmless N_2 and water. It is well known that NO reduction is possible only in a confined temperature range between 800 and 1100°C, the so-called 'temperature window'. Temperatures that are lower relative to the window stop the SNCR reactions, while higher temperatures oxidize the injected ammonia to NO and even higher NO_x emissions can be observed. The efficiency of the SNCR process varies between 30 and 80% and depends on several factors including temperature, NO_x level, the mixing of NH_3 into the flue gas, NH_3/NO molar ratio and residence time (Radojevic 1998). In addition, the presence of CO in the flue gas shifts the temperature window down to lower temperatures (Saario, Ylitalo, and Oksanen 2008). From the above, it is obvious that the SNCR system should be finely tuned in order to reduce NO in the flue gases effectively. Otherwise, if the mixing between NH_3 and NO is not proper and/or if the injected NH_3 follows a path outside the optimum temperature window, not only will SNCR fail to reduce NO to the desired level, but an appreciable amount of NH_3, an equally harmful substance, will also be released into the environment (ammonia slip).

In this study, the boiler is equipped with an SNCR system consisting of nine injections in total that feed a mixture of NH_3 and air into the flue gas. From them, eight injections are at the level of 7.5 m (see Figures 2 and 3), from which two are on the front wall and six are shared between the two side walls, and the last one is on the rear wall at a level of 6.5 m (the jet that can be seen in Figure 4(a,b) originates from this injection). The target of this work is to optimize the NH_3 distribution between those inlets so that NO_x emissions are minimized, while ammonia slip is kept to an acceptable level. At the design point the distribution between all the SNCR injections is uniform. How much the outlet ammonia is allowed to increase in order to improve the NO emissions is defined by the so-called decision makers, who are engineers with in-depth technical knowledge of the subject.

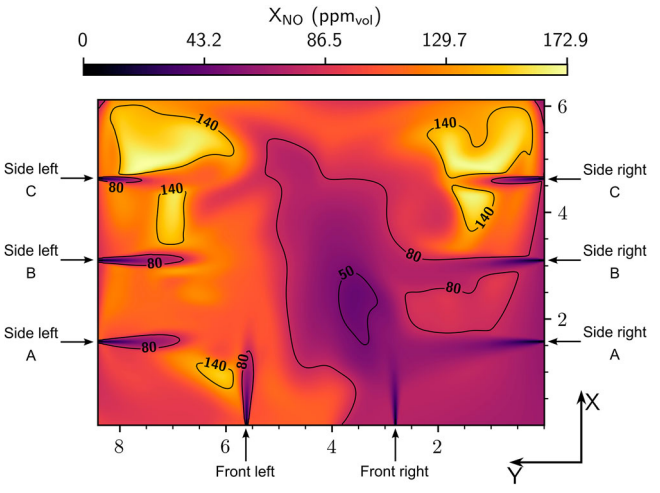

Figure 2. Contour of the NO volume fraction at the design point over the $z = 7.5$ m slice plane (viewed from the top).

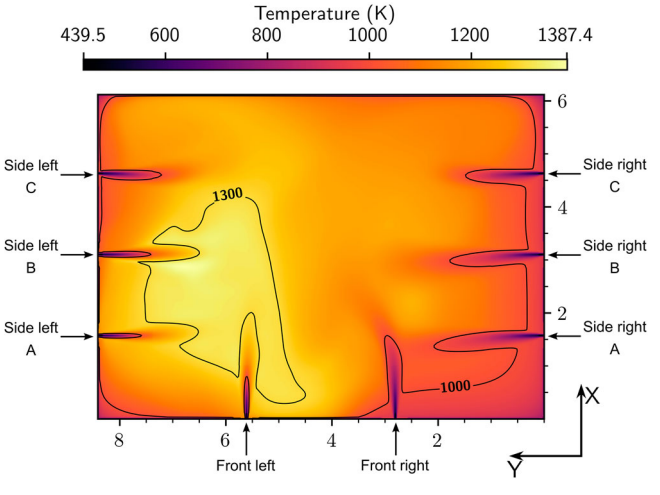

Figure 3. Temperature contour at the design point over the $z = 7.5$ m slice plane (viewed from the top).

3. Mathematical modelling

In the optimization process, for any given distribution of NH_3 between the ammonia inlets, the amounts of NO and NH_3 at the outlet should be calculated. Since pollutant (NO and NH_3) concentrations are very small compared to other species present in the flue gas mixture, it is assumed that they do not affect the main flow variables and the major species concentrations. Therefore, it suffices to calculate them in a post-processing fashion. Hence, the modelling of the BFBB comprises two separate stages: the reactive flow modelling and the emissions modelling. Since the design parameters of the optimization are the NH_3 concentrations in the ammonia jet inlets, only the post processing emission calculator will run during the optimization. Based on this, since this article focuses on the optimization, the first modelling stage will be discussed in brief.

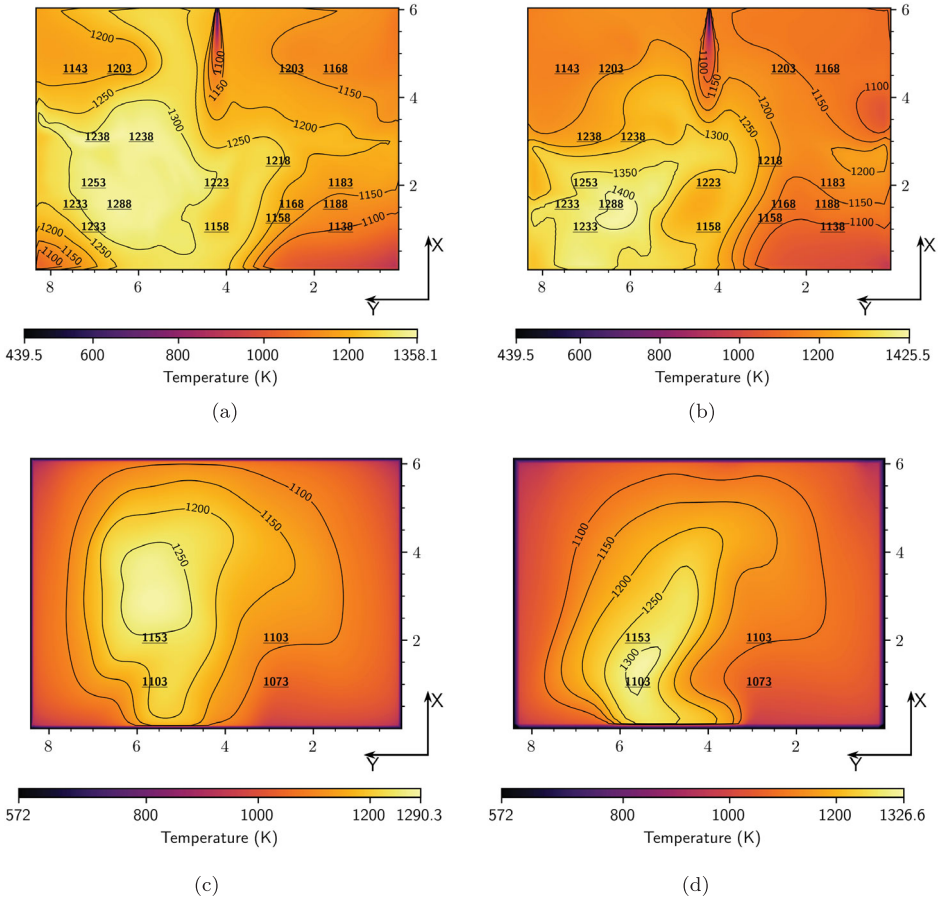

Figure 4. Temperature contours over the slice planes at $z = 6.5$ m and $z = 10$ m. Figures on the right and the underlined bold numbers on top of all the figures are CFD and experimental results, respectively, from the work of Saario, which are reported in Saario, Ylitalo, and Oksanen (2008) and Saario (2008). (a) Solution with OpenFOAM® (present) at $z = 6.5$ m; (b) Solution from Saario *et. al.* at $z = 6.5$ m; (c) Solution with OpenFOAM® (present) at $z = 10$ m; and (d) Solution from Saario *et. al.* at $z = 10$ m.

3.1. Reactive flow modelling

To model the BFBB, the Favre-averaged equations for the compressible, turbulent, reactive flow were solved using the open source software OpenFOAM®. Apart from the continuity, Navier–Stokes and the energy equation, a convection–diffusion equation is solved for any species mass fraction that is present in the gaseous mixture, except for N_2, which is set so that the sum of the species mass fractions amounts to one. As for the turbulence, although in previous studies of the same boiler the realizable k–ε model had been used successfully—see Saario, Ylitalo, and Oksanen (2008) and Saario and Oksanen (2008) and the references therein—in this study, the standard k–ε model (Launder and Spalding 1983) is used, because it was observed to be more stable. For more information on the turbulent reactive flow equations, see *e.g.* Poinsot and Veynante (2005). The reactions are modelled using the four-step Lindstedt and Jones reaction mechanism (Jones and Lindstedt 1988) and the turbulence–chemistry interaction is modelled with the Eddy Dissipation Combustion Model (EDCM) (Magnussen and Hjertager 1976), which was programmed by the authors. The radiation is modelled using the finite volume discrete ordinates method (Raithby and Chui 1990) to solve the radiative transport equation, in combination with the weighted-sum of grey gases model (Smith, Shen, and Friedman 1982) to calculate the gas-phase absorption coefficient.

The boundary conditions for this simulation can be found in Saario (2008). However, in the work of Saario, a constant heat flux boundary condition with a uniform value of $-500\,\mathrm{Wm}^{-2}$ was used for the refractory walls of the boiler. Since in practice the heat flux to the boiler walls is not uniform, it was here considered more accurate to solve for the wall heat transfer instead, through an approximate 1-D model. More specifically, the refractory wall boundary condition is derived from the following equation:

$$\mathrm{U}\,(T_w - T_\infty) = Q_r - k\nabla T, \tag{1}$$

where U is the so-called wall U-value, or thermal transmittance, set at 0.6 ($\mathrm{Wm}^{-2}\mathrm{K}^{-1}$), in order to match the experimentally calculated heat losses from the respective walls, T_w is the temperature of the inner wall, T_∞ is the ambient temperature, set at 298 K, Q_r (Wm^{-2}) is the incident radiation on the wall calculated from the radiation model, and k ($Wm^{-1}K^{-1}$) is the thermal conductivity of the flue gases.

The geometry is discretized using a grid sufficiently fine for the present purposes consisting of 3.2 million cells. Keep in mind that the grid used here is an order of magnitude finer than the one used previously in Saario (2008). As a solver, a custom built modification of the reactingFoam solver is used. The convection terms are modelled using a second-order upwind scheme and the diffusion terms are discretized applying a second-order central-differencing scheme.

3.2. Emission modelling

The nitrogen species reactions inside the boiler are modelled using a computationally economical, global, two-step reaction mechanism:

$$\mathrm{NH_3 + O_2 \longrightarrow NO + H_2O + 0.5\,H_2} \tag{r1}$$

$$\mathrm{NH_3 + NO \longrightarrow N_2 + H_2O + 0.5\,H_2}. \tag{r2}$$

Here, as proposed by Saario, Ylitalo, and Oksanen (2008), the kinetic parameters developed by Brink, Kilpinen, and Hupa (2001) and Duo, Dam-Johansen, and Østergaard (1992) will be used in the lower ($z \leq 3.65$ m) and upper ($z > 3.65$ m) parts of the boiler, respectively. The NO and NH_3 species concentrations are calculated by solving a steady-state transport equation for each one, *i.e.*

$$\frac{\partial}{\partial x_i}\left(\bar{\rho}\widetilde{u}_i\widetilde{Y}_k\right) = \frac{\partial}{\partial x_i}\left(\left(\bar{\rho}D + \frac{\mu_t}{\mathrm{Sc}_t}\right)\frac{\partial \widetilde{Y}_k}{\partial x_i}\right) + \bar{S}_k \quad \text{for } k = 1, 2, \tag{2}$$

where $\bar{\rho}$ is the time-averaged density, $\widetilde{u}_i$ is the Favre-averaged velocity component in the direction i, $\widetilde{Y}_k$ is the Favre-averaged mass fraction of species k, D is the diffusion coefficient of the solved species in the mixture, which is considered constant and set at $1.43 \times 10^{-4}\,\mathrm{m^2s^{-1}}$, Sc_t is the turbulent Schmidt number set at 0.7 and $\bar{S}_k$ is the time-averaged production rate of species k. $\bar{S}_k$ is given by

$$\bar{S}_k = \sum_{r=1}^{N_r} M_k\left(\nu''_{k,r} - \nu'_{k,r}\right)\bar{\omega}_{\mathrm{eff},r}, \tag{3}$$

where N_r is the number of reactions, $\bar{\omega}_{\mathrm{eff},r}$ is the effective progress rate of the reaction r, which is dependent on the reaction mechanism and the combustion model considered, M_k is the molecular mass of species k and, finally, $\nu''_{k,r}$ and $\nu'_{k,r}$ are the corresponding stoichiometric coefficients for species k in the reaction r on the product and reactant sides. Here, the effective reaction rates are calculated using the Partially Stirred Reactor (PaSR) combustion model (Chomiak 1990; Chomiak and Karlsson 1996) in place of the Eddy Dissipation Concept (EDC) (Magnussen 2005), which was used in Saario (2008). PaSR is based on a similar concept to EDC, considering that reactions occur in a part of the computational cell. It also takes into account finite rate chemistry, similarly to EDC, which is

important here since the nitrogen species reactions are in general slow (*i.e.* the chemical timescale is comparable to the mixing timescale). The main reason for selecting PaSR is that its steady-state implementation is much faster than that of EDC, since it does not require the integration of an ODE system for each cell of the domain in order to calculate the reaction source terms. At the same time, PaSR has recently been shown to be of comparable accuracy to the EDC model and has been used successfully in various studies (Li *et al.* 2017; Fortunato *et al.* 2018). According to this model, the (effective) progress rate can be calculated as

$$\bar{\omega}_{\mathrm{eff},r} = \kappa \bar{\omega}_{\mathrm{ch},r}, \tag{4}$$

where κ is the volumetric fraction of the reacting part of the cell and $\bar{\omega}_{\mathrm{ch},r}$ is the 'laminar' progress rate of reaction r. In Equation (4) the rate $\bar{\omega}_{\mathrm{ch},r}$ is calculated using the law of mass action, *i.e.*

$$\bar{\omega}_{\mathrm{ch},r} = k_{f,r} \prod_{l=1}^{N} c_l^{\left(\eta'_{l,r}+\eta''_{l,r}\right)}, \tag{5}$$

where $k_{f,r}$ is the forward reaction rate given by the Arrhenius law, c_l is the molar concentration of species l, $\eta'_{l,r}$ and $\eta''_{l,r}$ are the rate exponents for the reactant and product species, respectively, and N is the number of species present in reaction r. In addition, the reactive volume fraction κ can be calculated as

$$\kappa = \frac{\tau_{\mathrm{ch}}}{\tau_{\mathrm{ch}} + \tau_{\mathrm{mix}}}, \tag{6}$$

where τ_{ch} and τ_{mix} are the chemical and mixing timescales, respectively. Here, the NH_3 production rate diagonal Jacobian element is used for the calculation of τ_{ch} as follows:

$$\tau_{\mathrm{ch}}^{-1} = -\frac{\partial f_{\mathrm{NH_3}}}{\partial C_{\mathrm{NH_3}}}, \tag{7}$$

where $f_{\mathrm{NH_3}}$ is the production rate of NH_3 ($\mathrm{kmol\,m^{-3}s^{-1}}$) and $C_{\mathrm{NH_3}}$ ($\mathrm{kmol\,m^{-3}}$) is the molar concentration of NH_3 in the mixture. The τ_{mix} is given by

$$\tau_{\mathrm{mix}} = C_{\mathrm{mix}} \sqrt{\frac{\mu_{\mathrm{eff}}}{\rho \varepsilon}}, \tag{8}$$

where $C_{\mathrm{mix}} = 0.5$ is used.

Although the PaSR model is in the official OpenFOAM® repositories, it is reimplemented by the authors, since OpenFOAM® uses a different chemistry time scale than the one in Equation (7). The species transport equations for the NH_3 and NO are solved in a segregated way using a custom-built, OpenFOAM® based solver keeping all the other species concentrations (apart from N_2, which is set so that the sum of the species mass fractions is equal to one) and the flow variables constant. The convection term is discretized using a first order upwind scheme, while the diffusion term is discretized applying a second-order central-differencing scheme.

4. Optimization

From Section 2, it can be inferred that, for this problem, there is not a single optimum solution, but rather a set of optima (a Pareto set). Each member of this set is better in terms of one of the pollutants NO or NH_3, but worse in terms of the other. Here, multiobjective optimization (MOO) is applied in order to identify this set. To achieve this, the optimal ammonia concentration distributions between the SNCR injections are being searched for, while the injected air–NH_3 mixture mass flux from each injection feed is kept constant. In addition, the total injected ammonia is constrained so that it does

Table 1. Optimization cases solved.

Case	$\dot{m}_{NH_3,max}$ (kg s^{-1})	$X_{NH_3,max}$ (ppm$_{vol}$)
MOO	0.0093	15
Case-I	0.0046	15
Case-II	0.0046	6.1

not surpass the capacity of the feeding system, which is twice the value at the current design point. Moreover, for the NH_3 emission, a limit of 15 ppm$_{vol}$ should be guaranteed based on knowledge from the decision makers. All in all, the expected result from the optimization process is an approximation of the part of the Pareto set with NH_3 values less than 15 ppm$_{vol}$.

Apart from this, two additional optimization cases will be studied, which will be referred to from now on as 'Case-I' and 'Case-II'. Case-I optimizes the distribution between the SNCR injections while keeping the total injected ammonia at most the same as the current design point. This case is of significant importance, since boiler operators prefer to keep the injected ammonia as small as possible for cost reasons. For this case, the upper limit for the NH_3 at the outlet is set at 15 ppm. Case-II has the same total ammonia injection constraint, but a more stringent NH_3 outlet limit, equal to the current design point's NH_3 emissions. This is also an interesting case, since it proposes a solution that reduces NO emissions without any cost in exchange (neither the total SNCR injection or the NH_3 at the flue gases outlet are increased). It can be observed that both Case-I and Case-II are Single Objective Optimization (SOO) cases, where the second objective (outlet NH_3) is converted into a constraint.

4.1. Formulation of the problem

Consider a minimization problem. Since the target is the simultaneous minimization of the NO and NH_3 emissions, the objective function vector $\boldsymbol{f}(\boldsymbol{x})$ is given by

$$\boldsymbol{f}(\boldsymbol{x}) = \left(f_{NO}(\boldsymbol{x}), f_{NH_3}(\boldsymbol{x})\right)^T, \tag{9}$$

where $f_{NO}(\boldsymbol{x})$ and $f_{NH_3}(\boldsymbol{x})$ are the mole weighted averages of the mole fractions of NO and NH_3 in the flue gas at the boiler outlet, respectively. For the SOO cases, Case-I and Case-II, only $f_{NO}(\boldsymbol{x})$ is included in (9). The design variable vector $\boldsymbol{x}$ is given by

$$\boldsymbol{x} = (Y_1, Y_2, Y_3, \ldots, Y_9)^T, \tag{10}$$

where Y_i stands for the mass fraction (kg/kg) of NH_3 in the ith SNCR injection. The feasible set, S, is defined as

$$\begin{aligned} S = \Big\{ \boldsymbol{x} \in \mathbb{R}^9 \mid 0 \le Y_i \le Y_{max} \le 1, \text{ for } i = 1, 2, 3, \ldots, 9, \\ c_1(\boldsymbol{x}) = \dot{m}_{flow} \sum_{i=1}^{9} Y_i - \dot{m}_{NH_3,max} \le 0, \\ c_2(\boldsymbol{x}) = f_{NH_3}(\boldsymbol{x}) - X_{NH_3,max} \le 0 \Big\}, \end{aligned} \tag{11}$$

where $\dot{m}_{flow}$ is the mixture mass flux in each injection ($\dot{m}_{flow} = 0.1313$ kg s^{-1}), $\dot{m}_{NH_3,max}$ is the maximum allowed total NH_3 injected into the boiler and $X_{NH_3,max}$ stands for the maximum allowed NH_3 emission at the outlet. The design variable upper bounds (Y_{max}) are set equal to $\dot{m}_{NH_3,max}/\dot{m}_{flow}$, by virtue of constraint c_1. A compact representation of the optimization cases solved and their respective constraints can be found at Table 1.

4.2. Multiobjective optimization

The most popular method for solving a multiobjective optimization problem is the weighting method (see *e.g.* Cohon [2004]) due to its simplicity in implementation and intuitiveness. According to this, the MOO problem is converted into a set of SOO problems by minimizing several convex combinations of the objectives. For example, here, 21 weight combinations were used and so the MOO problem was converted into a series of 21 SOO problems. Specifically, the following problem is solved using an even distribution of 21 weight combinations in the interval [0, 1]:

$$\begin{aligned} \min \quad & F = w_{\mathrm{NO}}\widehat{f_{\mathrm{NO}}}(\boldsymbol{x}) + w_{\mathrm{NH_3}}\widehat{f_{\mathrm{NH_3}}}(\boldsymbol{x}) \quad \text{with } w_{\mathrm{NO}}, w_{\mathrm{NH_3}} > 0, w_{\mathrm{NO}} + w_{\mathrm{NH_3}} = 1 \\ \text{s.t.} \quad & \boldsymbol{x} \in S, \end{aligned} \tag{12}$$

where min–max normalized objective functions are used, namely $\widehat{f_{\mathrm{NO}}}$ and $\widehat{f_{\mathrm{NH_3}}}$, in order to capture a better representation of the Pareto front. More precisely, $\widehat{f_{\mathrm{NO}}}$ and $\widehat{f_{\mathrm{NH_3}}}$ are given as

$$\widehat{f_{\mathrm{NO}}} = \frac{f_{\mathrm{NO}} - f_{\mathrm{NO}}^{\mathrm{U}}}{f_{\mathrm{NO}}^{\mathrm{N}} - f_{\mathrm{NO}}^{\mathrm{U}}}, \quad \widehat{f_{\mathrm{NH_3}}} = \frac{f_{\mathrm{NH_3}} - f_{\mathrm{NH_3}}^{\mathrm{U}}}{f_{\mathrm{NH_3}}^{\mathrm{N}} - f_{\mathrm{NH_3}}^{\mathrm{U}}} \tag{13}$$

where $(f_{\mathrm{NO}}^{\mathrm{U}}, f_{\mathrm{NH_3}}^{\mathrm{N}})$ and $(f_{\mathrm{NO}}^{\mathrm{N}}, f_{\mathrm{NH_3}}^{\mathrm{U}})$ are the objective function values obtained when a SOO of NO and NH_3 emissions, respectively, is performed. It should be noted here that the weighting method has two well known drawbacks—see Das and Dennis (1997). Firstly, it is not able to capture the non-convex regions of the Pareto set, and secondly, a uniform distribution of weights can lead to a highly non-uniform distribution of the Pareto set points in the objective space, especially if the Pareto set has some flat regions (*i.e.* with almost constant slope of the Pareto curve).

Another popular method for MOO is the ε-constraint method introduced by Haimes, Lasdon, and Wismer (1971), in which one of the objective functions is minimized while setting upper bounds on all the rest, having them act as constraints. This method is used in practice when solving the two additional cases described previously as Case-I and Case-II.

Although it is straightforward to combine the aforementioned methods with evolutionary algorithms, the SPEA2 (*i.e.* Strength Pareto Evolutionary Algorithm) method (Zitzler, Laumanns, and Thiele 2001) is used instead, mainly because with one EA run the whole Pareto set can be approximated. Moreover, SPEA2 encourages front spreading so that the elite set individuals are evenly distributed in the objective space.

4.3. Gradient-based optimization

4.3.1. Solution of SOO sub-problems with the gradient-projection method

The independent SOO problems resulting from the weighting method, as well as the SOO Case-I and Case-II, are solved using a modification of the steepest descend method, the Gradient-Projection Method (GPM). This is a primal, first derivative method that dates back to Rosen (1960), initially developed for linear constraints and then extended to handle nonlinear ones as well (Rosen 1961). The basic idea behind this method is to project the steepest descend direction onto a tangent to the active constraints subspace, remaining this way on the feasible side of the domain while improving the objective function at the same time. In this way, the algorithm produces feasible and continuously improved solutions at any iteration, until convergence.

Here, a brief description of the method follows. Let F be the function to be minimized. This algorithm keeps track of the active constraints, which belong to the so called active set, $\mathcal{A}_n$. GPM applies a movement

$$\boldsymbol{\Delta x} = \boldsymbol{x}_{n+1} - \boldsymbol{x}_n = -\eta\, \mathbf{P} \nabla F, \tag{14}$$

where η is a coefficient (step) and $\mathbf{P}$ is a projection matrix. $\mathbf{P}$ is calculated from the QR decomposition

of the matrix $\mathbf{N}$, whose columns are the active constraints' gradients. It is

$$\mathbf{N} = [\mathbf{Q}_1 \quad \mathbf{Q}_2] \begin{bmatrix} \mathbf{R} \\ \mathbf{0} \end{bmatrix} = \mathbf{Q}_1 \mathbf{R} \tag{15}$$

and

$$\mathbf{P} = \mathbf{Q}_2 \mathbf{Q}_2^{\mathrm{T}}. \tag{16}$$

Also an additional step, $\boldsymbol{\Delta x'}$, is taken in order to restore any lost feasibility because of the nonlinearity of the constraints, *i.e.*

$$\boldsymbol{\Delta x'} = -\mathbf{N} \left(\mathbf{N}^{\mathrm{T}} \mathbf{N} \right)^{-1} \boldsymbol{c}_a, \tag{17}$$

where $\boldsymbol{c}_a$ is the vector of active constraints. Here, the two steps given by (14) and (17) are combined into one, as proposed by Arora and Haug (1979; see also Haftka and Gürdal 2012, 179). In addition, during the iterations a constraint can be removed from the active set dependent on the sign of its first-order Lagrange multiplier approximations.

4.3.2. Calculation of the sensitivity derivatives

In this study, the discrete adjoint method is used for the calculation of the sensitivity derivatives. In this section, the implementation of the discrete adjoint method will be briefly presented. The adjoint method is a powerful and fast way (comparing with finite differences) to calculate the sensitivity derivatives of a PDE constrained problem. Here, the problem is constrained by the nitrogen species transport equations (2). In the following, F is the objective function to be minimized, $\boldsymbol{R}$ are Equations (2) in their discretized form (more precisely a column vector containing the residuals of the discretized equations), $\boldsymbol{Y}$ is a column vector containing the NH_3 and NO mass fractions at the centre of the cells, which are the unknowns of the direct problem, and $\boldsymbol{Y}_{\mathbf{NH_3,b}}$ are the mass fractions of ammonia at the SNCR inlets, which are the design variables of the optimization problem. In general, F is a function of the unknowns of the direct problem and the design variables, *i.e.*

$$F = F\left(\boldsymbol{Y}, \boldsymbol{Y}_{\mathbf{NH_3,b}}\right). \tag{18}$$

It can be observed that $\boldsymbol{Y}$ is an implicit function of the design variables, *i.e.* $\boldsymbol{Y} = \boldsymbol{Y}(\boldsymbol{Y}_{\mathbf{NH_3,b}})$, through Equations (2). So, a change in $\boldsymbol{Y}_{\mathrm{NH_3,b}}$ changes F by

$$\delta F = \frac{\partial F}{\partial \boldsymbol{Y}} \boldsymbol{\delta Y} + \frac{\partial F}{\partial \boldsymbol{Y}_{\mathbf{NH_3,b}}} \boldsymbol{\delta Y}_{\mathbf{NH_3,b}}. \tag{19}$$

The variations $\boldsymbol{\delta Y}$ and $\boldsymbol{\delta Y}_{\mathbf{NH_3,b}}$ can be related through the direct problem equations in their discrete form, $\boldsymbol{R}$, which should be satisfied at any design point. So,

$$\boldsymbol{R}\left(\boldsymbol{Y}, \boldsymbol{Y}_{\mathbf{NH_3,b}}\right) = 0 \Rightarrow \boldsymbol{\delta R} = \frac{\partial \boldsymbol{R}}{\partial \boldsymbol{Y}} \boldsymbol{\delta Y} + \frac{\partial \boldsymbol{R}}{\partial \boldsymbol{Y}_{\mathbf{NH_3,b}}} \boldsymbol{\delta Y}_{\mathbf{NH_3,b}} = 0. \tag{20}$$

Because of Equation (20), Equation (19) can be written as

$$\begin{aligned} \delta F &= \frac{\partial F}{\partial \boldsymbol{Y}} \boldsymbol{\delta Y} + \frac{\partial F}{\partial \boldsymbol{Y}_{\mathbf{NH_3,b}}} \boldsymbol{\delta Y}_{\mathbf{NH_3,b}} - \boldsymbol{A}^{\mathrm{T}} \left(\frac{\partial \boldsymbol{R}}{\partial \boldsymbol{Y}} \boldsymbol{\delta Y} + \frac{\partial \boldsymbol{R}}{\partial \boldsymbol{Y}_{\mathbf{NH_3,b}}} \boldsymbol{\delta Y}_{\mathbf{NH_3,b}} \right) \\ &= \left(\frac{\partial F}{\partial \boldsymbol{Y}} - \boldsymbol{A}^{\mathrm{T}} \frac{\partial \boldsymbol{R}}{\partial \boldsymbol{Y}} \right) \boldsymbol{\delta Y} + \left(\frac{\partial F}{\partial \boldsymbol{Y}_{\mathbf{NH_3,b}}} - \boldsymbol{A}^{\mathrm{T}} \frac{\partial \boldsymbol{R}}{\partial \boldsymbol{Y}_{\mathbf{NH_3,b}}} \right) \boldsymbol{\delta Y}_{\mathbf{NH_3,b}}, \end{aligned} \tag{21}$$

where $\boldsymbol{A}$ is a column vector containing the adjoint variables. Then $\boldsymbol{A}$ is chosen so that the $\boldsymbol{\delta Y}$ product term is discarded from Equation (21) by solving the following, so-called adjoint, equation:

$$\left(\frac{\partial \boldsymbol{R}}{\partial \boldsymbol{Y}}\right)^{\mathrm{T}} \boldsymbol{A} = \left(\frac{\partial F}{\partial \boldsymbol{Y}}\right)^{\mathrm{T}}, \tag{22}$$

or, if tensor notation is used,

$$\frac{\partial R_i}{\partial Y_j} A_i = \frac{\partial F}{\partial Y_j}, \tag{23}$$

where both indices i, j run through the unknowns of the problem at hand (*e.g.* the number of differential equations times the number of cells). Then, according to Equation (21), the sensitivity derivatives can be given from the relation

$$\frac{\delta F}{\delta Y_{\mathrm{NH_3,b},i}} = \frac{\partial F}{\partial Y_{\mathrm{NH_3,b},i}} - A_j \frac{\partial R_j}{\partial Y_{\mathrm{NH_3,b},i}}, \tag{24}$$

where here the indices i and j run through the design variables and the unknowns of the direct problem, respectively.

One can observe from Equations (23) and (24) that

$$\frac{\partial \boldsymbol{R}}{\partial \boldsymbol{Y}}, \quad \frac{\partial F}{\partial \boldsymbol{Y}}, \quad \frac{\partial F}{\partial \boldsymbol{Y}_{\mathbf{NH_3,b}}} \quad \text{and} \quad \frac{\partial \boldsymbol{R}}{\partial \boldsymbol{Y}_{\mathbf{NH_3,b}}}$$

should be calculated. Assume that the target is to minimize the NO emissions of the boiler. Then, the objective function can be defined as the mole weighted average of the NO mole fraction at the outlet

$$F = \frac{\displaystyle\int_{\mathrm{out}} \rho u_i n_i \frac{Y_{\mathrm{NO}}}{W_{\mathrm{NO}}}\, \mathrm{d}S}{\displaystyle\int_{\mathrm{out}} \frac{\rho u_i n_i}{W_{\mathrm{mix}}}\, \mathrm{d}S}, \tag{25}$$

where $P_{\mathrm{out}} = \int_{\mathrm{out}} \rho u_i n_i / W_{\mathrm{mix}}\, \mathrm{d}S$ is the outlet mixture mole flux, W_{mix} is the mixture molar mass, which is considered to be unaffected by NO concentration, and W_{NO} is the NO species molar mass. In Equation (23), the discrete form of Equation (25) is used, *i.e.*

$$F \approx \frac{1}{P_{\mathrm{out}}} \sum_{\mathrm{outlet},i} \phi_i \frac{Y_{\mathrm{NO},i}}{W_{\mathrm{NO}}}, \tag{26}$$

where ϕ_i and $Y_{\mathrm{NO},i}$ are the mass flux and the NO mass fraction of the outlet face with index i, respectively. Since at the outlet a zero-gradient boundary condition is used for the species, $Y_{\mathrm{NO},i} = Y_{\mathrm{NO},P_i}$, with Y_{NO,P_i} being the value at the centre of the cell neighbouring the face i. Now $\partial F/\partial \boldsymbol{Y}$ and $\partial F/\partial \boldsymbol{Y}_{\mathbf{NH_3,b}}$ can easily be calculated by differentiating Equation (26). In fact, it is easy to observe that here $\partial F/\partial \boldsymbol{Y}_{\mathbf{NH_3,b}}$ is a zero row vector. In a similar manner, after having formed $\boldsymbol{R}$, $\partial \boldsymbol{R}/\partial \boldsymbol{Y}$ and $\partial \boldsymbol{R}/\partial \boldsymbol{Y}_{\mathbf{NH_3,b}}$ are calculated by hand, differentiating the respective terms.

Afterwards, the adjoint code is programmed in the OpenFOAM® framework. The resulting adjoint equations are solved using a biconjugate-gradient block solver from the foam-extend project (https://sourceforge.net/projects/foam-extend/), which is a fork of OpenFOAM®.

Table 2. Evolutionary algorithm parameters.

Parents' population size	15
Offspring population size	40
Elite set size	26
Mutation probability	4%
Coding	Binary–Grey, 12 bits
Discretization accuracy	$\Delta Y \approx 0.0017$ wt%

4.4. Evolutionary algorithm optimization

In order to validate the optimization results, the MOO problem is also solved using an Evolutionary Algorithm (EA) through the generic EA based software platform 'EASY' (Giannakoglou 2008; Parallel CFD and Optimization Unit 2008). Although the EA based optimization of the problem presented in section 4.1 is also performed in Saario and Oksanen (2008), it is repeated here since some of the models used are different, and so the results are not anticipated to be exactly the same. The basic parameters of the EA run can be found in Table 2. Keep in mind that finding the best tuning of the EA is beyond the scope of this work.

In an attempt to improve the performance of the EA, the following changes in the setup over the previous work by Saario and Oksanen (2008) are performed.

- Here, the whole optimization process is automated and the problem is solved directly as a MOO problem using the SPEA2 technique to assign fitness values to the individuals (see also Section 4.2). In this way, the Pareto set is approximated with one EA run. In contrast, in the previous study, an interactive method was used together with an achievement scalarizing function to convert the problem from MOO to SOO, see Saario and Oksanen (2008) and the references therein.
- It can be observed that the calculation of the first of the constraints in Equation (11) does not require any CFD evaluation. This fact is smartly exploited to reduce the computational cost by bypassing the CFD solver run when the first constraint is strongly violated (more that 10%).
- In order to reduce the computational cost further, online trained metamodels are used to provide low cost approximations of the objective functions through the Inexact PreEvaluation (IPE) mode of the EASY software (Karakasis and Giannakoglou 2005; Giannakoglou 2002; Karakasis, Giotis, and Giannakoglou 2003). In this study, the metamodels are based on Radial Basis Function (RBF) networks. The inexact preevaluations start after having collected approximately 4000 successful evaluations in the database, a file written by EASY containing all the candidate solutions and their evaluations. This happens after 186 generations. From the 187th generation onwards, all the individuals are first evaluated using the metamodels and, after that, the best 6–16 of them are evaluated using the 'exact' CFD (OpenFOAM®) solver.

The EA runs are performed using 10 processors and continued until the algorithm has stopped finding better solutions. In the end, approximately 16,000 'exact' (CFD) evaluations and another 13,000 'inexact' ones are performed.

5. Results and discussion

5.1. Reactive flow modelling results

In order to validate the OpenFOAM® solver, the solution obtained is compared with experimental and CFD modelling results from the PhD work of Saario, who used a different, commercial, solver—see Saario (2008) and the references therein. Figure 5 plots the area-weighted average of the temperature as a function of boiler height up to $z = 13$ m, as modelled with OpenFOAM® in the present study, in comparison with the solution of Saario (2008). Although the solver, the mesh,

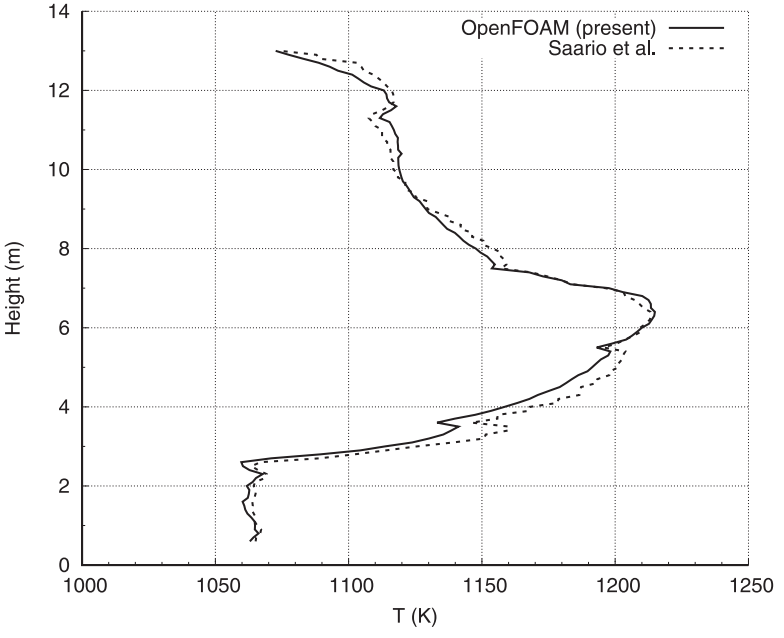

Figure 5. Area-weighted average of temperature as function of boiler height.

the refractory wall temperature boundary condition and the version of the k–ε model are different between the two boiler models, the average temperature differs by no more than 20 K. Figure 4 shows the temperature contours resulting from the reactive flow modelling with OpenFOAM® at the levels $z = 6.5$ and 10 m, in comparison with the CFD and experimental results from the work of Saario, reported in Saario, Ylitalo, and Oksanen (2008) and Saario (2008). From this figure, it can be seen that the temperature contours calculated here are rather similar to the ones reproduced from Saario's results. In addition, the locations of the temperature peaks of both CFD models are in close proximity. One difference between the two models is that the temperature peak of Saario's solution is higher (67.4 degrees higher at the $z = 6.5$ m level and 36.3 degrees higher at $z = 10$ m). As for the measurements, it can be seen that they are all well below the CFD results. This discrepancy can be attributed mainly to the fact that a bare unshielded thermocouple was used, which typically underestimates the temperature due to the radiation losses to the walls. For temperatures that prevail at the height $z = 6.5$ m, the error can be as much as 100 K (Kitto and Stultz 2005; Saario 2008). Nevertheless, refractory walls, which have a relatively high temperature, are used at this height, and so the radiation losses to them can be somewhat restrained. In fact, at a level of $z = 6.5$ m, the maximum differences between the CFD and the experimental results are in the order of 80–100 degrees and are observed in the hottest region of the slice, near the maximum temperature, as anticipated. However, in the rest of the slice, the differences are below 50 degrees, decreasing with decreasing temperature, as expected. At the higher level of $z = 10$ m, bigger deviations between the CFD and the experimental results are anticipated, since the bounding walls are composed of pipes carrying steam, and so they are much colder ($T = 572$ K) than the flue gases. Indeed, at this level, the differences between the CFD and the experimental results are in the order of 100 K. Anyway, the radiation losses of the pyrometer are difficult to calculate, and so those measurements can only be used as an indication of the temperature levels at different locations. All things considered, the OpenFOAM® model applied is able to predict the temperatures inside the BFBB reasonably well, in accordance with the CFD modelling and the experimental results of Saario.

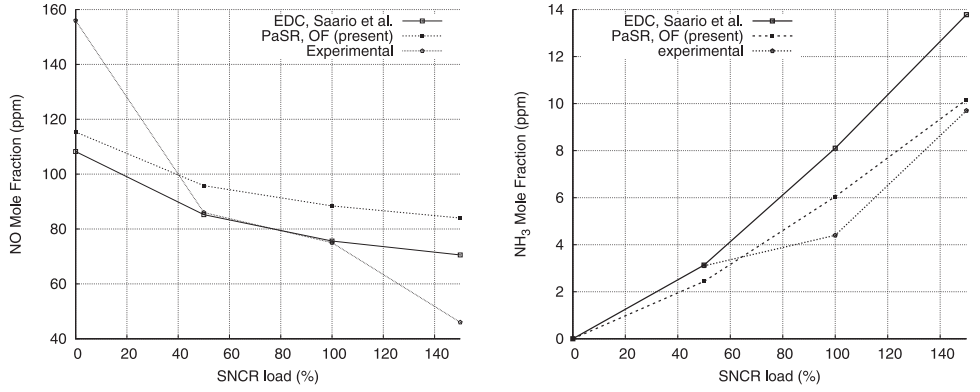

Figure 6. NO versus SNCR load (left), and NH_3 versus SNCR load (right).

5.2. Emission modelling results

Figure 6 shows this work's prediction of the NO and NH_3 emissions versus different SNCR loads in comparison with CFD predictions and the experimental results of Saario (Saario 2008; Saario, Ylitalo, and Oksanen 2008). Keep in mind that here the PaSR combustion model is used for the emission calculations instead of the EDC used in Saario (2008). Nevertheless, as far as the CFD results are concerned, they predict almost the same efficiencies for NO reduction with increasing SNCR load (see Figure 6 (left)). It can also be observed that both models underestimate the NO reduction at small and big SNCR loads, while for loads close to the design point, Saario's model gives a better match with the experiments. In contrast, for the NH_3 (see Figure 6 (right)), the modelling applied in this work provides generally a better match to the experimental results. The discrepancies between the CFD and experimental results are attributed mainly to the approximate nature of the RANS based model combined with a global mechanism. This type of models can only be expected to provide approximate and qualitatively correct predictions and trends for nitrogenous species pollutants (NO, NH_3) (Zahirović *et al.* 2010). Considering that this work deals with an industrial scale boiler in the context of optimization, with hundreds at least CFD based evaluations being performed, the cost of using a detailed mechanism in combination with LES or even RANS would have been prohibitive. Another source of error might be the simplified modelling of the bubbling bed. Besides CFD models, the experimental results are susceptible to several errors. Firstly, the measurement equipment manufacturer reports an error of 10%. In addition, measurements are taken from only one position in the middle of the flue gas channel. For more information about the measurements, see Saario (2008, 61). All in all, the model applied here is able to predict the emissions from the BFBB reasonably well, and so it is considered a credible tool for the evaluation of the different candidate solutions during optimization.

5.3. Verification of the sensitivity derivatives

The adjoint gradients are verified against Finite Difference (FD) derivative calculations using a forward difference formula with a step equal to 1×10^{-8}. As shown in Figure 7, the differences between the adjoint and the FD gradients are negligible.

5.4. Optimization results

Figure 8 shows the results obtained from all the optimization runs. It contains the elite set of the evolutionary algorithm, the results of the SOO problems resulting from the use of the weighting method and then optimized using the GPM and the two extra optimization cases considered here and also solved with the GPM, *i.e.* Case-I and Case-II. It can be observed that, for the weighting method, only

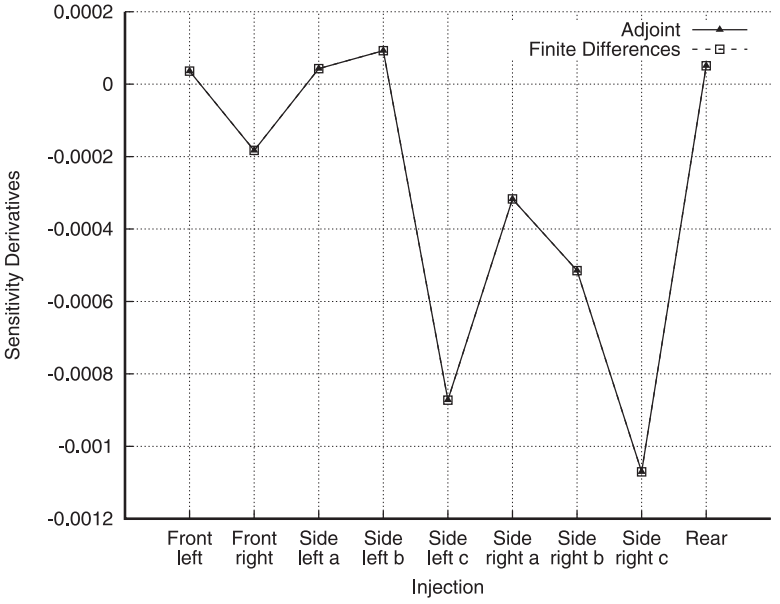

Figure 7. Comparison of adjoint versus finite differences gradient calculations.

18 points appear in the figure, while 21 different weight combinations were used. That is because, for $w_{NO} \geq 0.85$, the optimal solutions collapse onto the same point because the outlet NH_3 upper limit is reached. Also in Figure 8, the four points of most interest to the decision makers are marked as 'a', 'b', 'c' and 'd'. Points 'a' and 'b' are the weighting method solutions with the lowest NO emissions. Those points are rather significant, since NO reduction is the main target here. Additionally, points 'c' and 'd' are the solutions for Case-I and Case-II, respectively. Point 'a' gives the highest NO reduction (19.2%) from the design point. In return, it increases NH_3 emissions by 145.9% and also the injected NH_3 by 84.8%. Point 'b' decreases outlet NO by 16.7%, and increases the outlet NH_3 and the injected NH_3 by 104.9% and 54.3%, respectively. Point 'c' decreases NO by 14.5% with NH_3 emissions remaining marginally below the 15 ppm_{vol} limit, while not increasing the injected ammonia at all. Finally, point 'd' achieves an NO reduction of 8% without injecting more ammonia or increasing the ammonia emissions. One can also observe that points 'c' and 'd' essentially lie on the Pareto front which would be obtained with a stricter ammonia injection limit equal to the current design's value.

The representations of the Pareto front found by the gradient-projection method and the evolutionary algorithms are in general rather similar. One difference is that the points found when using the weighting method are a little biased towards the uninteresting, low NH_3/high NO end of the Pareto front, while the EA results with the SPEA2 method are more evenly distributed. Nevertheless, a satisfactory representation and distribution of Pareto points is still achieved when using the weighting method. This is because the Pareto set for this problem does not contain any non-convex or 'flat' regions. So it can be concluded that the weighting method is suitable and effective for the solution of the MOO problem here. Another difference is that the gradient-projection method, being exploitation oriented, has provided more refined solutions when compared with the exploration oriented evolutionary algorithms (see Figure 8). Moreover, after 16,000 exact and 13,000 inexact evaluations, the evolutionary algorithm could not provide any global optima with significantly improved performance over the GPM solutions. Even though this is not a guarantee that the GPM found the global optima, it means that, probably, the optima found by the GPM do not differ much in the objective space from the global ones. Therefore, it can be concluded that the danger of converging to local optima when using the GPM is of minor practical importance here.

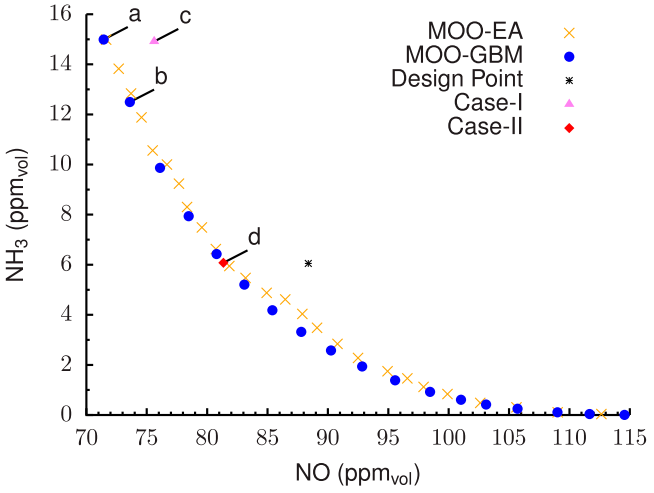

Figure 8. Optimization results in the objective function space. 'MOO-EA' is the solution to the MOO problem using evolutionary algorithms, 'MOO-GBM' is the solution to the MOO problem using the weighting method with the gradient-based method for the SOO subproblems, and Case-I and Case-II are the solutions to Case-I and Case-II using the gradient-projection method.

Figure 9 shows the representation of the solutions 'a', 'b', 'c' and 'd' in the design space. The figure reveals that the optimum distributions are far from the uniform distribution of the design point. It can also be seen that, at the optimum solutions, several of the constraints are binding. For example, for the solution 'a', five constraints are binding; four of them are the simple variable bounds and the fifth is the outlet NH_3, which is 15 ppm_{vol}. It is interesting to notice that all solutions of Figure 9 run with 'Front left', 'Side left a' and 'Side left b' injections completely turned off. Also, the injection 'Front right' is turned off in 'a' and 'c' and almost turned off in 'b' and 'd'. In addition, all of the solutions propose that the injected NH_3 from the 'Side left c' injection should be increased. A similar finding was also noticed by Saario and Oksanen (2008).

In order to interpret the results physically, the contours of NO at levels $z = 7$ and 7.5 m, as well as the temperature contour at the level of $z = 7.5$ m are plotted in Figures 10, 2 and 3, respectively. Figures 2 and 10 reveal that most of the NO is formed in the rear part of the boiler, close to the left and right walls with even higher concentrations at the left walls. That is why mainly the 'Side left c' but also the 'Side right c' injections have higher concentrations than the design point in the optimum solutions. In addition, Figure 3 shows that the temperature close to the left front part of the boiler is higher than it should be for the SNCR to perform properly. Also, close to the right front part, the temperature is less than the optimum SNCR temperature owing to the impact of two of the SNCR jets, which are much colder than the average flue gases in the region. That is why all the optimum solutions run with 'Front left', 'Side left a' and 'Side left b' injections turned off and with at most a very small NH_3 concentration at the 'Front right' injection.

5.5. Adjoint method efficiency

The cost of solving the adjoint equations and calculating the gradients is similar to one direct emission calculation problem. So the cost of one optimization cycle employing the adjoint method is equal to two emission calculation problems (since both the direct and the adjoint problem have to be solved), while this increases to $n + 1$ direct problems if FDs are used ($n = 9$ here). Keep in mind that, in areas close to the maximum allowed NH_3 constraint, one extra adjoint calculation is needed for the NH_3 gradient, thus increasing the optimization cost to three emission calculation problems per optimization round. From the above, it is apparent that there is an enormous performance benefit (70–80%) when using the adjoint method over FDs.

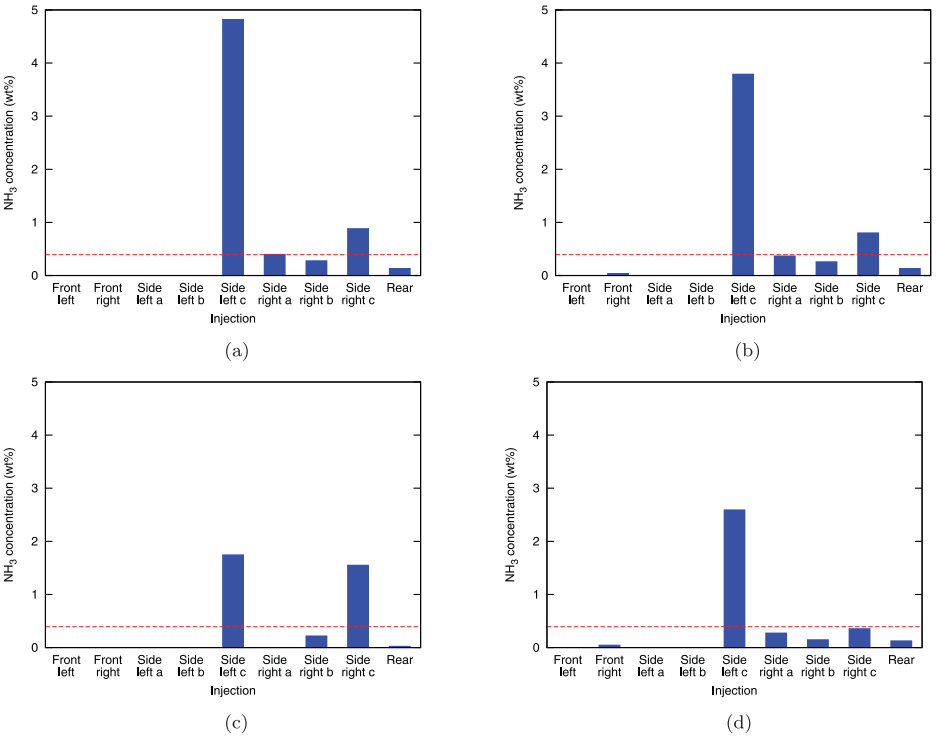

Figure 9. Representation of the solutions 'a', 'b', 'c' and 'd' (see also Figure 8) in the design space. The dashed-line represents the uniform distribution of NH_3 concentration at the design point. (a) Solution 'a': $f_{NO} = 71.4\,ppm_{vol}$, $f_{NH_3} = c_2 = 15\,ppm_{vol}$ (active), $c_1 = 0.0085\,kg\,s^{-1}$ (inactive); (b) Solution 'b': $f_{NO} = 73.6\,ppm_{vol}$, $f_{NH_3} = c_2 = 12.5\,ppm_{vol}$ (inactive), $c_1 = 0.0071\,kg\,s^{-1}$ (inactive); (c) Solution 'c': $f_{NO} = 75.6\,ppm_{vol}$, $f_{NH_3} = c_2 = 14.9\,ppm_{vol}$ (inactive), $c_1 = 0.0046\,kg\,s^{-1}$ (active); and (d) Solution 'd': $f_{NO} = 81.3\,ppm_{vol}$, $f_{NH_3} = c_2 = 6.1\,ppm_{vol}$ (active), $c_1 = 0.0046\,kg\,s^{-1}$ (active).

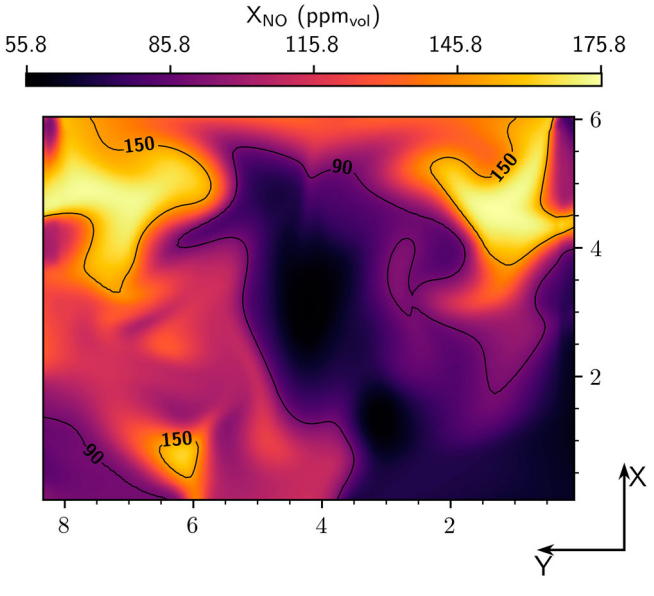

Figure 10. Contour of the NO volume fraction at the design point over the $z = 7$ m slice plane (viewed from the top).

5.6. Gradient-projection method efficiency

The SOO problems solved with the GPM converged in about 140 optimization cycles. Every cycle comprises the solution to the direct problem, the gradient calculation of the objective function and the gradient calculation of the nonlinear constraint c_2. So the equivalent cost of each optimization round is about three direct problems and the optimization cost for each point in Figure 8 is about 420 direct problems. In practice, the cost is actually much less than that since the gradient of the constraint c_2 is only calculated when the current iterate approaches the constraint isosurface within some user specified tolerance. All the SOO subproblems are independent of each other and so are solved in parallel with the exception of the first two SOO problems needed for the normalization of the objectives. Considering the 16,000 exact and 13,000 inexact evaluations performed during the EA optimization, the enormous performance benefit when using gradient-based methods becomes evident.

6. Conclusions

Here, the discrete adjoint method was successfully applied in this industrial combustion case. In the end, it was found to be rather efficient and accurate for the sensitivity derivatives calculation, providing a great speed-up over the use of FDs.

The weighting method, which was used to convert the MOO problem into a series of SOO problems, was able to provide a satisfactory distribution of Pareto set points. This can be attributed to the shape of the Pareto front for this specific application. In addition, the gradient-projection method proved to be satisfactorily efficient in solving the resulting SOO problems. The efficiency of the optimization can be further improved if a second order gradient-based method is used utilizing the Hessian or an approximation thereof (*e.g.* using the Broyden-Fletcher-Goldfarb-Shanno [BFGS] algorithm). All in all, the gradient-based method applied in this study was more efficient in terms of computational time, providing at the same time more refined solutions than the evolutionary algorithm. This fact encourages the use of adjoint-based optimization in other industrial combustion cases as well.

In the end, a 19.2% decrease in the NO emissions could be achieved at the expense of increasing the injected SNCR ammonia and also the NH_3 emissions at the outlet (which still remained at an acceptable level). Also, according to the result for Case-II, an 8% improvement in NO emissions can be achieved at no extra cost. Ultimately, which solution will finally be selected will be decided by the decision makers based on the increase of the outlet as well as the injected NH_3 that they can tolerate in exchange for the NO reduction. For general guidance, the 'Side left c' and the 'Side right c' concentrations should be increased, while the injections 'Front left', 'Front right', 'Side left a' and 'Side left b' should be turned off.

It should be noted that the exact gains, if the proposed solutions are actually used, depend on the accuracy of the modelling. Here, as seen in Section 5.2, the predictions are only qualitatively correct. In practice, this means that, while the proposed NH_3 distributions would probably decrease the NO emissions, the decrease percentages will not be exactly equal to those predicted by the model. This fact does not detract from the usefulness of the applied optimization, since the results are still a valuable indication of the changes that should be made to reduce the emissions. In order to be on the safe side, the proposed solutions should be tested further by experiments before they are applied in practice and/or a solution well below the upper NH_3 limit (*e.g.* Case-II), which still decreases NO, can be selected.

Although the results produced here are specific to this geometrical configuration, the method and the tools developed and used in this work are general and can be tailored and applied to other optimization problems relating to industrial boilers as well. Finally, it is worth mentioning that in cases optimizing the more fundamental parameters of the boiler, such as the geometry or the speed of the secondary air injections, the reactive flow solver should also be coupled to the optimization process,

since a change in those parameters would also change the flow field and the major species concentrations in the boiler. This means that the reactive flow solver should also be run during the evaluation of each candidate solution. In addition, it should also be differentiated for the calculation of the required sensitivity derivatives.

Acknowledgments

The authors would like to thank Professor Kyriakos Giannakoglou for fruitful discussions and constructive comments on the optimization part of this article. Thanks also to the CSC-IT Center for Science in Espoo, Finland, for providing the required computational resources for the successful realization of this work.

Disclosure statement

No potential conflict of interest was reported by the author(s).

Funding

Financial assistance from Valmet Technologies Oy, the EES doctoral school of the Academy of Finland, and Tampere University of Technology (Tampereen Teknillinen Yliopisto) is gratefully acknowledged.

References

Arora, J. S., and E. J. Haug. 1979. *Applied Optimal Design: Mechanical and Structural Systems*. New York: Wiley–InterScience.

Braman, Kalen, Todd A. Oliver, and Venkat Raman. 2015. "Adjoint-Based Sensitivity Analysis of Flames." *Combustion Theory and Modelling* 19 (1): 29–56.

Brink, Anders, Pia Kilpinen, and Mikko Hupa. 2001. "A Simplified Kinetic Rate Expression for Describing the Oxidation of Volatile Fuel-N in Biomass Combustion." *Energy & Fuels* 15 (5): 1094–1099. doi:10.1021/ef0002748.

Chomiak, Jerzy. 1990. *Combustion: A Study in Theory, Fact and Application*. London: Abacus Press/Gordon & Breach.

Chomiak, Jery, and Anders Karlsson. 1996. "Flame Liftoff in Diesel Sprays." *Symposium (International) on Combustion* 26 (2): 2557–2564. doi:10.1016/S0082-0784(96)80088-9.

Cohon, Jared L. 2004. *Multiobjective Programming and Planning*. Vol. 140 in the series Mathematics in Science and Engineering. Mineola, NY: Dover Publications.

Dal Secco, Sandro, Olivier Juan, Myriam Louis-Louisy, Jean-Yves Lucas, Pierre Plion, and Lynda Porcheron. 2015. "Using a Genetic Algorithm and CFD to Identify Low NO_x Configurations in An Industrial Boiler." *Fuel* 158: 672–683. doi:10.1016/j.fuel.2015.06.021.

Das, Indraneel, and John E. Dennis. 1997. "A Closer Look At Drawbacks of Minimizing Weighted Sums of Objectives for Pareto Set Generation in Multicriteria Optimization Problems." *Structural Optimization* 14 (1): 63–69.

Duo, W., K. Dam-Johansen, and K. Østergaard. 1992. "Kinetics of the Gas-Phase Reaction Between Nitric Oxide, Ammonia and Oxygen." *The Canadian Journal of Chemical Engineering* 70 (5): 1014–1020.

Fortunato, Valentina, Andreas Giraldo, Mehdi Rouabah, Rabia Nacereddine, Michel Delanaye, and Alessandro Parente. 2018. "Experimental and Numerical Investigation of a MILD Combustion Chamber for Micro Gas Turbine Applications." *Energies* 11 (12): Article ID 3363. doi:10.3390/en11123363.

Giannakoglou, K. C. 2002. "Design of Optimal Aerodynamic Shapes Using Stochastic Optimization Methods and Computational Intelligence." *Progress in Aerospace Sciences* 38 (1): 43–76. doi:10.1016/S0376-0421(01)00019-7.

Giannakoglou, Kyriakos. 2008. "EASY (the Evolutionary Algorithms System)." http://velos0.ltt.mech.ntua.gr/EASY/.

Giles, Michael B., and Niles A. Pierce. 2000. "An Introduction to the Adjoint Approach to Design." *Flow, Turbulence and Combustion* 65 (3–4): 393–415.

Haftka, Raphael T., and Zafer Gürdal. 2012. *Elements of Structural Optimization*. Vol. 11 in the series Solid Mechanics and Its Applications. Dordrecht, The Netherlands: Springer Science & Business Media.

Haimes, Y. Y., Leon S. Lasdon, and David A. Wismer. 1971. "On a Bicriterion Formation of the Problems of Integrated System Identification and System Optimization." *IEEE Transactions on Systems, Man and Cybernetics* 1 (3): 296–297. doi:10.1109/TSMC.1971.4308298.

Jameson, Antony. 1988. "Aerodynamic Design Via Control Theory." *Journal of Scientific Computing* 3 (3): 233–260.

Jameson, Antony, Luigi Martinelli, and N. A. Pierce. 1998. "Optimum Aerodynamic Design Using the Navier–Stokes Equations." *Theoretical and Computational Fluid Dynamics* 10 (1-4): 213–237.

Jameson, Antony, and James Reuther. 1994. "Control Theory Based Airfoil Design Using the Euler Equations." In *Proceedings of the 5th Symposium on Multidisciplinary Analysis and Optimization*, Paper No. AIAA-94-4272-CP. Reston, VA: AIAA. doi:10.2514/6.1994-4272.

Janiga, G., and D. Thévenin. 2007. "Reducing the CO Emissions in a Laminar Burner Using Different Numerical Optimization Methods." *Proceedings of the Institution of Mechanical Engineers, Part A: Journal of Power and Energy* 221 (5): 647–655.

Jones, W. P., and R. P. Lindstedt. 1988. "Global Reaction Schemes for Hydrocarbon Combustion." *Combustion and Flame* 73 (3): 233–249.

Karakasis, M. K, and K. C. Giannakoglou. 2005. "Metamodel-Assisted Multi-Objective Evolutionary Optimization." In *Proceedings of the Conference on Evolutionary and Deterministic Methods for Design, Optimization and Control with Applications to Industrial and Societal Problems (EUROGEN 2005)*. Athens, Greece: National Technical University of Athens. http://eurogen2001.ltt.mech.ntua.gr/research/confs/3_075.pdf.

Karakasis, M. K., A. P. Giotis, and K. C. Giannakoglou. 2003. "Inexact Information Aided, Low-Cost, Distributed Genetic Algorithms for Aerodynamic Shape Optimization." *International Journal for Numerical Methods in Fluids* 43 (10–11): 1149–1166.

Kitto, J. B., and S. C. Stultz. 2005. *Steam: Its Generation and Use*. 41st ed. Akron, OH: Babcock & Wilcox.

Launder, Brian Edward, and Dudley Brian Spalding. 1983. "The Numerical Computation of Turbulent Flows." *Numerical Prediction of Flow, Heat Transfer, Turbulence and Combustion* 1983: 96–116. doi:10.1016/B978-0-08-030937-8.50016-7.

Lemke, Mathias, Julius Reiss, and Jörn Sesterhenn. 2014. "Adjoint Based Optimisation of Reactive Compressible Flows." *Combustion and Flame* 161 (10): 2552–2564.

Li, Zhiyi, Alberto Cuoci, Amsini Sadiki, and Alessandro Parente. 2017. "Comprehensive Numerical Study of the Adelaide Jet in Hot-Coflow Burner by Means of RANS and Detailed Chemistry." *Energy* 139: 555–570.

Liu, Xingrang, and R. C. Bansal. 2014. "Integrating Multi-Objective Optimization with Computational Fluid Dynamics to Optimize Boiler Combustion Process of a Coal Fired Power Plant." *Applied Energy* 130: 658–669.

Magnussen, Bjorn F. 2005. "The Eddy Dissipation Concept—A Bridge Between Science and Technology." In *Proceedings of the 2005 ECCOMAS Thematic Conference on Computational Combustion*. http://folk.ntnu.no/ivarse/edc/BFM_ECOMAS2005_Lisboa.pdf.

Magnussen, B. F., and B. H. Hjertager. 1976. "On Mathematical Modeling of Turbulent Combustion with Special Emphasis on Soot Formation and Combustion." *Symposium (International) on Combustion* 16 (1): 719–729. doi:10.1016/S0082-0784(77)80366-4.

Nadarajah, Siva, and Antony Jameson. 2000. "A Comparison of the Continuous and Discrete Adjoint Approach to Automatic Aerodynamic Optimization." In *Proceedings of the 38th Aerospace Sciences Meeting and Exhibit*, Paper No. AIAA-2000-0667. Reston, VA: AIAA. doi:10.2514/6.2000-667.

Parallel CFD and Optimization Unit. 2008. *EASY v2.0 Users' Manual*. Athens, Greece: National Technical University of Athens. http://velos0.ltt.mech.ntua.gr/EASY/.

Pironneau, Olivier. 1982. "Optimal Shape Design for Elliptic Systems." In *System Modeling and Optimization: Proceedings of the 10th International Federation for Information Processing Conference*, 42–66. Berlin: Springer. doi:10.1007/BFb0006123.

Poinsot, Thierry, and Denis Veynante. 2005. *Theoretical and Numerical Combustion*. 2nd ed. Philadelphia, PA: R.T. Edwards.

Radojevic, Miroslav. 1998. "Reduction of Nitrogen Oxides in Flue Gases." *Environmental Pollution* 102 (1, Supplement 1): 685–689. doi:10.1016/S0269-7491(98)80099-7.

Raithby, G. D., and E. H. Chui. 1990. "A Finite-Volume Method for Predicting a Radiant Heat Transfer in Enclosures with Participating Media." *ASME Transactions—Journal of Heat Transfer* 112: 415–423. https://ui.adsabs.harvard.edu/abs/1990ATJHT.112..415R/abstract.

Risio, Benedetto, Frank Blum, Jens Hetzer, Alexander Berreth, and Uwe Hein. 2005. "Towards An Innovative Virtual Optimisation Machine for the Power Industry." *Progress in Computational Fluid Dynamics, an International Journal* 5 (7): 398–405. https://www.deepdyve.com/lp/inderscience-publishers/towards-an-innovative-virtual-optimisation-machine-for-the-power-bPCdUSbLVC.

Rosen, Jo Bo. 1960. "The Gradient Projection Method for Nonlinear Programming. Part I. Linear Constraints." *Journal of the Society for Industrial and Applied Mathematics* 8 (1): 181–217.

Rosen, J. B. 1961. "The Gradient Projection Method for Nonlinear Programming. Part II. Nonlinear Constraints." *Journal of the Society for Industrial and Applied Mathematics* 9 (4): 514–532.

Saario, Ari. 2008. "Mathematical Modeling and Multiobjective Optimization in Development of Low-Emission Industrial Boilers." Doctor of Technology Thesis, Tampere University of Technology, Hervanta, Finland. http://urn.fi/URN:NBN:fi:tty-200903021021.

Saario, Ari, and Antti Oksanen. 2008. "Computational Fluid Dynamics and Interactive Multiobjective Optimization in the Developement of Low-Emission Industrial Boilers." *Engineering Optimization* 40: 869–890.

Saario, Ari, Matti Ylitalo, and Antti Oksanen. 2008. "Comparison of Global Ammonia Chemistry Mechanisms in Biomass Combustion and Selective Noncatalytic Reduction Process Conditions." *Energy & Fuels* 22: 297–305.

Salahi, Sara. 2012. "Automated Process and Geometry Design Optimization of a Coal Combustion Reactor." PhD diss., Rutgers University Graduate School, New Brunswick. https://doi.org/doi:10.7282/T3MG7NJ6.

Smith, T. F., Z. F. Shen, and J. N. Friedman. 1982. "Evaluation of Coefficients for the Weighted Sum of Gray Gases Model." *Journal of Heat Transfer* 104 (4): 602–608.

Thévenin, Dominique, and Gábor Janiga. 2008. *Optimization and Computational Fluid Dynamics*. Berlin: Springer. doi:10.1007/978-3-540-72153-6.

Weller, Henry G., Gavin Tabor, Hrvoje Jasak, and Christer Fureby. 1998. "A Tensorial Approach to Computational Continuum Mechanics Using Object-Oriented Techniques." *Computers in Physics* 12 (6): 620–631.

Zahirović, Selma, Robert Scharler, Pia Kilpinen, and Ingwald Obernberger. 2010. "Validation of Flow Simulation and Gas Combustion Sub-Models for the CFD-Based Prediction of NO_x Formation in Biomass Grate Furnaces." *Combustion Theory and Modelling* 15 (1): 61–87.

Zitzler, Eckart, Marco Laumanns, and Lothar Thiele. 2001. "SPEA2: Improving the Strength Pareto Evolutionary Algorithm." TIK-Report 103. Computer Engineering and Networks Laboratory (TIK) Department of Electrical Engineering Swiss Federal Institute of Technology (ETH) Zürich. https://pdfs.semanticscholar.org/6672/8d01f9ebd0446ab346a855a44d2b138fd82d.pdf.